Submillimeter fMRI reveals a layout of dorsal visual cortex in macaques, remarkably similar to New World monkeys

Qi Zhu[a,1] and Wim Vanduffel[a,b,c,d,1]

[a]Laboratory of Neuro- and Psychophysiology, Department of Neurosciences, KU Leuven, 3000 Leuven, Belgium; [b]Athinoula A. Martinos Center for Biomedical Imaging, Massachusetts General Hospital, Charlestown, MA 02129; [c]Department of Radiology, Harvard Medical School, Boston, MA 02144; and [d]Leuven Brain Institute, Department of Neurosciences, KU Leuven, 3000 Leuven, Belgium

Edited by David C. Van Essen, Washington University School of Medicine in St. Louis, St. Louis, MO, and approved December 14, 2018 (received for review March 30, 2018)

The macaque dorsal occipital cortex is generally thought to contain an elongated third visual area, V3d, extending along most of the rostral border of area V2. In contrast, our submillimeter retinotopic fMRI maps (0.6-mm isotropic voxels, achieved by implanted phased-array receive coils) consistently show three sectors anterior to V2d. The dorsal (mirror image) sector complies with the traditional V3d definition, and the middle (nonmirror image) sector with V3A. The ventral (mirror image) sector bends away from V2d, as does the ventrolateral posterior area (VLP) in marmosets and the dorsolateral posterior area (DLP) in owl monkeys, and represents the entire contralateral hemifield as V3A does. Its population-receptive field size, however, suggests that this ventral sector is another area at the same hierarchical level as V4d. Hence, contrary to prevailing views, the retinotopic organization of cortex rostral to V2d differs substantially from widely accepted models. Instead, it is evolutionarily largely conserved in Old and New World monkeys given its surprisingly similar overall visuotopic organization.

high-resolution fMRI | retinotopy | primate | V3 | V4

The visuotopic organization of primate third-tier visual areas has been a longstanding source of controversy, even ∼40 y after their discovery (1–5). The current most widely used model in macaques (model 1, Fig. 1*A*) proposes an elongated V3 extending along most of the rostral V2 border. This V3 contains a split upper (UVF) and lower visual field (LVF) representation mirroring that of V2 in its ventral (V3v) and dorsal portion (V3d), respectively. Occasionally, a small gap has been reported in the middle of the V3d of some subjects, thereby interrupting the representation of the lower vertical meridian (LVM) at the anterior V3d border (6). Rostral to V3d, another area, V3A, represents the entire contralateral hemifield. Initially, V3A was described with a LVM at its posterior border with V3d, and an upper vertical meridian (UVM) at its rostral border with the fourth visual area (V4) (7). The most widely adopted model (model 1, Fig. 1*A*), however, shows an UVF posteriorly and a LVM bordering V4 anteriorly in V3A (6). This textbook model contrasts sharply with models based on and from New World monkeys (e.g., Fig. 1 *B* and *C*), with the latter assigning cortex rostral to V2d to two different areas: a dorsomedial area (DM) representing the entire contralateral hemifield and another area curving rostrally away from V2 [ventrolateral posterior area (VLP) in marmosets and dorsolateral posterior area (DLP) in owl monkeys, respectively].

These contradicting models fueled a fierce debate concerning the general topographic layout of the dorsal visual cortex in primates. On one hand, a DM-like organization of dorsal third-tier visual areas is proposed in all primates, with an alternative schematic for the macaque (Fig. 1*D*). The latter model 4 suggests that the most medial part of the V3d of model 1 should be combined with the upper quadrant of V3A and PO/V6 to form area DM, and the most ventral part of V3d should be combined with the lower quadrant of V3A and V3v into the area VLP (2, 8). On the other hand, a V3d-like organization, based on combined evidence from Old and New World monkeys, is proposed for all primates. In this model 5 (Fig. 1*E*), area V3d is wedged between DM and V2d.

To resolve this ongoing debate, we acquired high-resolution (0.6-mm isotropic voxels) phase-encoded retinotopic maps in three awake macaques using implanted phased-array coils (9, 10) and contrast agent-enhanced fMRI (11). This revealed large-scale but fine-grained topographic information across the brain, close in resolution to most microelectrode retinotopic mapping studies (0.3 ∼ 0.5 mm in depth, but 0.8 ∼ 1 mm between penetrations). Although recent fMRI studies revealed detailed retinotopic maps of the macaque visual cortex (12–14), they all seemed to confirm the widely accepted model 1 in Fig. 1*A* (but see ref. 2). In contrast, our results revealed a substantially different organization of cortex immediately anterior to V2d that largely reconciles macaque and New World monkey models.

Results

Three Retinotopically Distinct Sectors Immediately Anterior to Macaque V2d. Fig. 2*A* displays retinotopic maps from the top half of the left hemisphere of a representative subject (M1). The iso-polar angle and iso-eccentricity contours are drawn in thin colored lines, and different field signs are indicated using slightly transparent shadings. Based on field sign reversals, which signify opposite directions of the polar angle gradient between adjoining

Significance

The primate visual system encompasses >30 visual areas. Characterizing each area, and the interactions between them, is a prerequisite to understanding the visual system. This fundamental task, however, requires a precise parcellation of the visual cortex. Nonetheless, already at the earliest visual processing stages, i.e., just rostral to V2, the number and exact definition of areas are heavily contested. Here, we map the macaque visual cortex using fMRI at unprecedented high resolution. We show a substantially different retinotopic organization of dorsal third and fourth visual areas in macaques compared with widely accepted models, yet a remarkably similar layout in Old and New World monkeys. This organization largely reconciles most reported discrepancies concerning the visuotopic organization of nonhuman primate caudo-dorsal occipital cortex.

Author contributions: Q.Z. and W.V. designed research; Q.Z. performed research; W.V. performed the surgeries; Q.Z. analyzed data with input from W.V.; and Q.Z. and W.V. wrote the paper.

The authors declare no conflict of interest.

This article is a PNAS Direct Submission.

[1]To whom correspondence may be addressed. Email: qi.zhu@kuleuven.be or wim@nmr.mgh.harvard.edu.

This article contains supporting information online at www.pnas.org/lookup/suppl/doi:10.1073/pnas.1805561116/-/DCSupplemental.

Published online January 23, 2019.

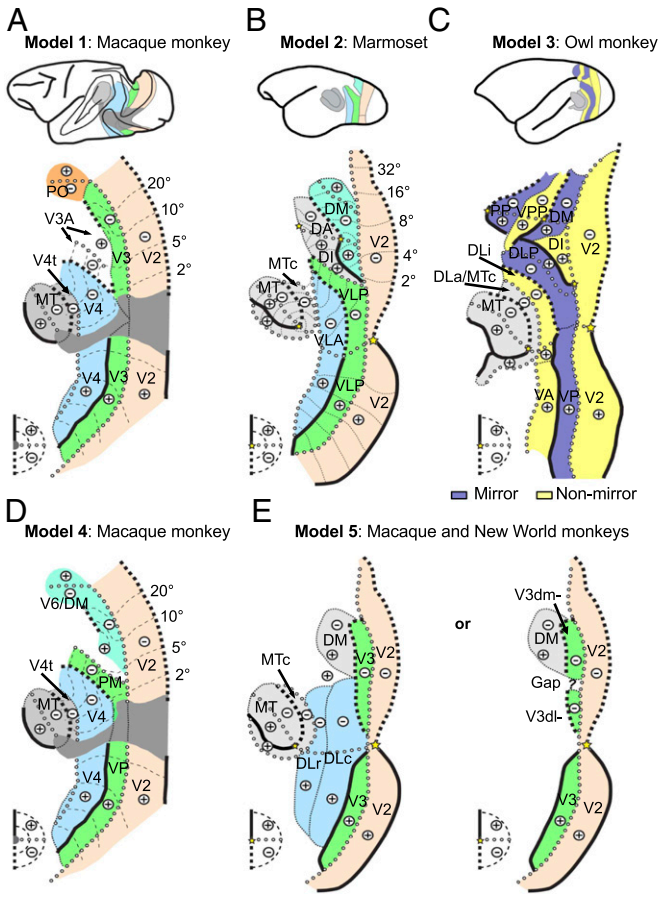

Fig. 1. Different visuotopic models of early visual areas in Old and New World monkeys. (*A*) Most widely accepted macaque model based on Gattass et al. (1, 6). (*B*) New World marmoset model based on Rosa and Tweedale (8) and Angelucci and Rosa (2). (*C*) New World owl monkey model (3). (*D*) Reinterpretation of macaque model 1 in *A* by Rosa and Tweedale (8) and Angelucci and Rosa (2) based on the marmoset model. (*E*) Model of Kaas and coworkers for both macaque and New World monkeys. Thin dashed lines are drawn for the anterior borders of DLc and DLr since visual field representations are difficult to discern from the results of Stepniewska and Kaas (29) and Stepniewska et al. (27). See *SI Appendix* for abbreviations. (*A*, *B*, and *D*) Republished with permission of Royal Society, from ref. 8; permission conveyed through Copyright Clearance Center, Inc. (*C*) Modified from ref. 3. (*E*, *Left*) Model reproduced from ref. 27 by permission of Oxford University Press. (*E*, *Right*) V3d model reproduced with permission from ref. 4.

areas with a congruent eccentricity gradient (or vice versa), several areal borders can be readily identified. The V1d/V2d border can be recognized as a LVM (red "a" in Fig. 2*A*) along a clear transition in field sign and a reversal of polar angle progression along the caudo-rostral axis between the two regions. Another LVM (red "b" in Fig. 2*A*) can be recognized along the prelunate gyrus and forms the posterior V4 border, in agreement with the prevailing V4 macaque model (Fig. 1*A*). Between V2 and V4, two mirror image sectors (R1 and R2, colored in blue in Fig. 2*A*) can be seen immediately rostral to V2d, with a gap (R3, nonmirror image, colored in red) containing an UVF representation located at the anterior bank of the lunate sulcus (*SI Appendix*, Fig. S1) separating them. The gap has been sporadically reported and has been regarded as a simple interruption of V3d (1, 4, 6, 13, 14) in the scheme corresponding to a combination of R1 and R2. However, our results show that these two sectors cannot comprise a single visuotopic area and even belong to different hierarchical levels.

Sector R1 (putative V3d). R1 shares a horizontal meridian (HM) with V2d caudally and a LVM (red "c" in Fig. 2*A*) with the nonmirror R3 sector, rostrally. Hence R1 represents only the LVF, at least within the lunate sulcus, and most likely corresponds to the most dorsal portion of V3d of model 1 (Fig. 1*A*) (but not V6, as discussed in detail in *SI Appendix*).

Sector R2 (putative DLP). R2, on the other hand, shares an UVM (red "d" in Fig. 2*A*) caudally with R3 and a LVM (red "b" in Fig. 2*A*) with V4 rostrally. Hence, R2 represents the entire contralateral hemifield. R2 also bends away from V2d, exactly as does VLP in marmosets (Fig. 1*B*). However, R2 is distinct from marmoset's VLP since the UVF representation dorsal to VLP is assigned to a different dorsointermediate area (DI) by Rosa and Tweedale (15). Instead, it rather resembles DLP, with its full hemifield and mirror image field sign, as described in New World owl monkeys (Fig. 1*C*). Theoretically, the dorsomedial part of R2 (green hatched area "c" in Fig. 2*C*) could also fit V3A from the macaque model 1 (Fig. 1*A*), as both R2 and V3A possess similar visual field representations and cortical locations. However, in that case, the most ventrolateral portion of R2 (red "a" in Fig. 2*C*) belongs to part of V3d while the UVF representation of R3 (red "b" in Fig. 2*C*) has to be included in V3A. This requires the unlikely combination of two regions with different field signs in one area (red and blue regions indicated by arrows "b" and "c" in Fig. 2*C*). Moreover, the UVF will be represented twice ("c" and "b"), which is unlikely within a single retinotopic area. Therefore, we regard a single-area DLP, as in the New World owl monkeys, as the most parsimonious explanation for R2, despite the strikingly lower magnification factor in the UVF compared with its LVF representation.

Sector R3 (putative V3A). The nonmirror sector R3 contains a representation of the entire contralateral hemifield, with a LVF (R3−) represented dorsomedially at the annectant gyrus and an UVF (R3+) represented ventrolaterally at the anterior bank of the lunate sulcus (Fig. 2*B*), remarkably similar to the V3A originally described by Van Essen and Zeki (7) [note that Van Essen and Zeki (7) had already offered the possibility that V3A might border V2d rostrally (see their figure 14)]. R3 is also similar to DM as proposed by Lyon and Kaas (16, 17) in both Old and New World

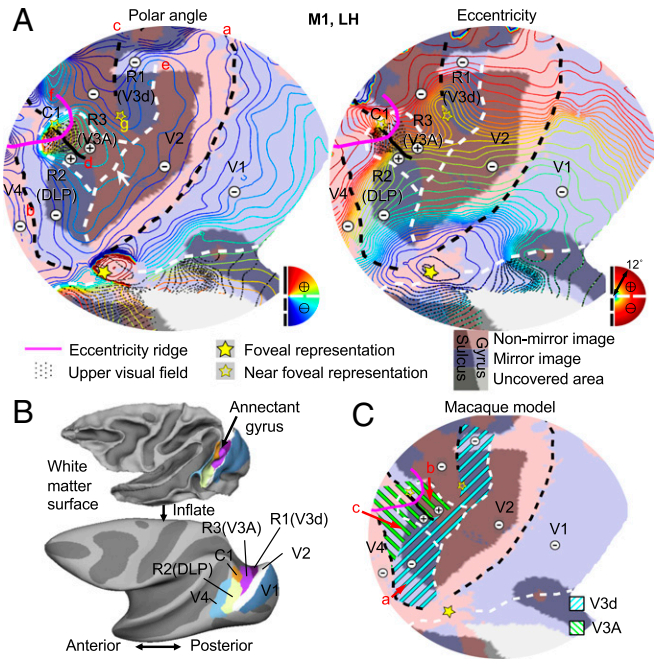

Fig. 2. Retinotopic organization of macaque dorsal areas of subject M1. (*A*) Polar angle and eccentricity maps (colored iso-contour lines) are displayed on the field sign map (red and blue shadings correspond to nonmirror and mirror image representations, respectively) of the left hemisphere (LH). (*B*) Areal outlines are shown on folded and inflated surfaces. (*C*) Reconciling results in *A* with existing macaque monkey models. The eccentricity of the open yellow star (g) corresponds to 2.6°.

monkeys. The UVF representation (R3+), however, abuts V2d directly, unlike DM in the recent schematics of Kaas et al. (4, 16, 17) (Fig. 1*E*). Instead, R3+ is more similar to DM+ proposed by Allman and Kaas (18) and by Rosa and Schmid (19). The more dorsomedial part of this sector shares a (near) center of gaze (yellow "g" in Fig. 2*A*) with R1 (V3d), around which near-central iso-eccentricity lines are clearly wrapped. The LVF representation (R3−) resembles VPP−, and the UVF representation (R3+) resembles DI+ as described by Sereno et al. (3) for owl monkeys, insofar as they represent the same quadrant and have the same nonmirror field sign (Fig. 1*C*). Unlike owl monkeys, however, we find no evidence for the UVF representations VPP+ and DM+, which should appear lateral to the center of gaze. Rostral to R3 (V3A) and dorsomedial to R2 (DLP), an eccentricity ridge (red "f" in Fig. 2*A*) is wrapped around another central representation (near C1 in Fig. 2*A*). This ridge aligns well with the transitions of visual field sign at the dorsomedial border of R2 and the rostral border of R3, thereby separating a small cluster of areas (C1) from both R2 and R3. In most hemispheres (*SI Appendix*, Figs. S2–S3), this C1 cluster contains a double representation of the entire contralateral hemifield and hence consists of more than one visual area. C1 will not be discussed further, except to say that it appears similar to PP in owl monkeys (3) (Fig. 1*C*). C1 might also overlap with a histologically defined intermediate area as the latter area was identified at the same location (20).

Consistent retinotopic layout across six hemispheres. The topographic organization described in detail for the left hemisphere of M1 is surprisingly consistent across all six hemispheres (*SI Appendix*, Figs. S2–S3). Only the right hemisphere of M3 shows no pronounced gap (nonmirror sector) immediately anterior to V2d. In general, our results point to an organization for dorsal visual cortex significantly differing from macaque models 1 and 5. This organization resembles that seen in New World monkeys (Fig. 1 *B* and *C*), except that different quadrants are combined to form areas with a complete contralateral visual field representation.

Population Receptive Field Sizes in R2 (DLP) and R1 (V3d). To objectively evaluate the various models, we estimated Population Receptive Field (pRF) sizes within each voxel (21) (Fig. 3). More specifically, we tested whether R2 and R1 belong to V3d as predicted by the classical macaque models 1 and 5. Alternatively, they consist of different areas (i.e., DLP and V3d, respectively), as suggested by our high-resolution retinotopic maps. The results show that pRF size increases with eccentricity for all areas and that pRF size at higher eccentricities increases from caudal (e.g., V2d) to rostral areas (e.g., V4d). Furthermore, pRF size at high eccentricities of R2 is much larger than that of R1 in every subject (Fig. 3).

A linear mixed-effect analysis of the pRF data showed that a model with a common intercept but separate slope terms best describes the data [Bayesian information criterion (BIC) = 479.09], compared with the simpler (BIC = 497.53) and more complex models (BIC = 495.09) (*SI Appendix*, *Methods*). Hence, slopes were compared across areas to quantify areal differences in pRF size

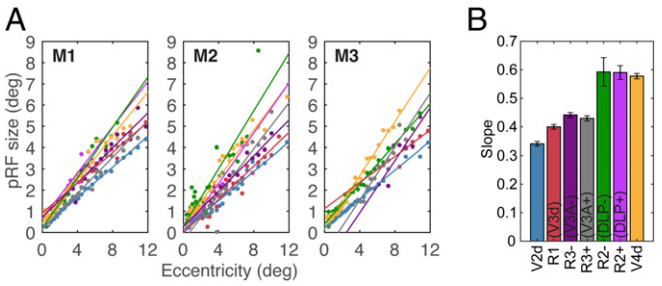

Fig. 3. The pRF sizes of all dorsal visual areas discussed in the present study. (*A*) Individual pRF sizes as a function of eccentricity. (*B*) Slope estimates (mean and SEM across subjects) from the best-fitted linear mixed-effect model. The color codes indicated in *B* are also used in *A*.

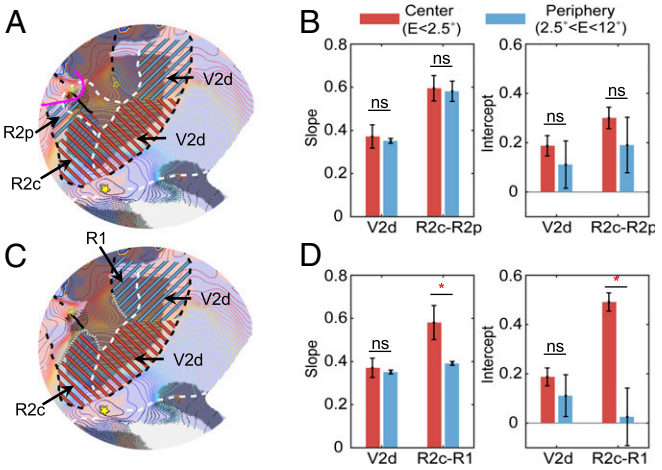

Fig. 4. Different pRF sizes in R1 (V3d) and R2 (DLP). (*A* and *B*) Slope and intercept estimates in central R2 (R2c) and V2d (red hatching in *A*) compared with their peripheral counterparts (R2p and V2d) (blue hatching in *A*). (*C* and *D*) Slope and intercept estimates in central R2 (R2c) and V2d (red hatching in *C*) compared with R1 (V3d) and peripheral V2d (blue hatching in *C*). *P < 0.05; ns, P > 0.05. Bars and error bars, mean and SEM across subjects.

(Fig. 3*B*). The best model provided an excellent fit of the data, explaining 94% of the variance (Adjusted $R^2 = 0.941$).

A pairwise comparison of the slopes showed that pRF size is smallest in V2d and largest in V4d [V2d < V3d < V4d, F's > 14.53, P's < 10^{-4}, false discovery rate (FDR) corrected], consistent with previous findings (6, 15, 22–24). There is no difference between the slopes of the two quadrants of R3 (V3A) [$F(1, 487) = 1.1$, $P = 0.34$, FDR corrected]. Importantly, the slope of R3+ is significantly smaller compared with R2+ [$F(1, 487) = 41.18$, $P < 0.005$, FDR corrected], adding to the field sign-based evidence that these are two independent upper quadrants. Moreover, R3's slopes are significantly larger than those of V2d and R1 (V3d) (F's > 7, P's < 0.01, FDR corrected) (see also *SI Appendix*, Fig. S4), but smaller than V4d (F's > 145, P's < 10^{-4}, FDR corrected). The slopes of the two R2 quadrants are indistinguishable [$F(1, 487) < 1$, $P = 0.968$, FDR corrected]. Critically, they are significantly larger than those of R1 (V3d) (F's > 14, Ps < 10^{-3}, FDR corrected) (see also *SI Appendix*, Fig. S4*A*), but equal to that of V4d (F's < 1, Ps > 0.6, FDR corrected), suggesting that R2 is likely at the same hierarchical level as V4, rather than being part of V3d.

The macaque models 1 and 5 consider only the more ventrolateral part of R2 as part of V3d (blue hatched area "a" in Fig. 2*C*), whereas the more dorsomedial part belongs to V3A (green hatched area "c" in Fig. 2*C*). Therefore, we divided R2 into two parts and compared their respective pRF sizes with R1. In Fig. 4 *A* and *B*, the pRF sizes in the central (eccentricity < 2.5°) and peripheral portions (2.5° < eccentricity < 12°) of R2 (DLP) were statistically compared using two linear mixed-effect models and V2d as a reference (*SI Appendix*, *Methods*). Both models showed highly similar results (F's < 1.3, Ps > 0.2) for the central and peripheral portions of R2 (DLP). Furthermore, differences in slopes or intercepts between the central and peripheral representations are indistinguishable for R2 (DLP) and V2d (two-way interaction, F's < 1, Ps > 0.7). In Fig. 4 *C* and *D*, a similar comparison was made between R1 (V3d) and the central portion of R2 (R2c). In this case, both the slope and intercept estimates of R2c are significantly larger than in R1 (V3d) (F's > 6, P's < 0.02), and these differences significantly exceed those between central and peripheral V2d [two-way interaction: slope, $F(1, 215) = 3.97$, $P = 0.0477$; intercept, $F(1, 215) = 8.72$, $P = 0.0035$]. Moreover, the same distinction between R2c and R1 (V3d) is obtained when much smaller eccentricity values are taken as the cutoff [e.g., 1°, two-way interaction between intercept estimates, $F(1, 184) = 7.39$, $P = 0.0072$]. Hence, these findings cannot be attributed to a larger area being assigned to R2c

(DLPc) versus R1 (V3d) by using a 2.5° eccentricity cutoff. These data add to the evidence that R2 (DLP) is quantitatively different from R1 (V3d) and strongly argue against an elongated V3d, as proposed in macaque models 1 and 5.

Intriguingly, despite the intrinsic intersubject variability of pRF data, highly similar pRF results are obtained using low-resolution (1- to 1.25-mm isotropic voxels) retinotopic data from eight additional subjects (*SI Appendix*, Fig. S6). The only caveat is that these low-resolution data do not provide enough voxels to separate the upper and lower quadrants of DLP and V3A, hence high-resolution experiments are required to distinguish such small quadrant representations.

Does R2 (DLP) Fit the New World Monkey Model? To test whether the LVF quadrant of R2 (R2−/DLP−) may be considered a continuation of V3v as in a New World monkey model (Fig. 1*B*), we also compared pRF sizes between R2− (DLP−) and V3v (Fig. 5). Compared with dorsal areas, the retinotopic organization of ventral areas is less complex, and areal boundaries can be straightforwardly delineated along field sign reversals (Fig. 5*A*). The pRF size results show consistent areal differences across subjects (*SI Appendix*, Fig. S5), and a linear mixed-effect model with fixed and random effects including both common-intercept and separate-slope terms for each area best fitted the data (BIC = 402.87), compared with the simpler (BIC = 464.89) and more complicated models (BIC = 433.76). The slope estimates (Fig. 5*B*) from the best model indicated similar pRF sizes in ventral and dorsal V2 and V4, respectively (F's < 1, Ps > 0.6, FDR corrected), highly consistent with previous single-cell recording studies (6, 22, 25, 26). Similarly, the slope of V3v equals that of R1 (V3d) [$F(1, 606) = 2.47$, $P = 0.144$, FDR corrected], but is significantly smaller than that of R2− (DLP−) [$F(1, 606) = 13.66$, $P < 0.001$, FDR corrected]. Similar results were also observed in the low-resolution data (*SI Appendix*, Fig. S6). This suggests that R2 (DLP) is likely a higher level area relative to V3v.

Discussion

Our submillimeter retinotopic mapping of macaque cortex demonstrated multiple retinotopically organized areas immediately rostral to V2d. These areas are collectively termed third-tier visual areas based on their adjacency to V2 (18); however, they likely belong to different hierarchical levels. The most dorsomedial area (R1) contains a mirrored visual field representation of V2d, and its receptive field size equals that of V3v, exactly as previously described for V3d. Rostral to the middle sector of V2d, a nonmirror image area (R3) is located at the annectant gyrus with a visual field representation surprisingly similar to V3A as initially described by Van Essen and Zeki (7). The most lateral area (R2) curves away from V2d and contains a representation of the entire contralateral hemifield, exactly fitting DLP, as described for New World owl monkeys (3). Its central portion directly abuts V2d and is separated from V3d by a gap, whereas its pRF size is significantly larger than that of V3d (R1) and V3v. Hence, R2 is most likely not part of V3d, nor a LVF continuation of V3v. Receptive field size in both its quadrants, however, is quite similar to that of V4, suggesting that R2 (DLP) is probably a fourth-, rather than third-level, visual area. The high-resolution pRF data were surprisingly similar to those obtained from eight subjects scanned at lower resolution. Together, the results reveal a topographic organization for macaque dorsal visual areas rostral to V2d that substantially differs from the most widely accepted macaque models. The overall retinotopic organization, however, is surprisingly similar to the New World monkey.

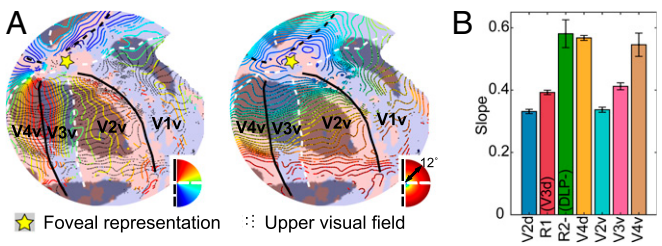

Fig. 5. Different pRF sizes in V3v and R2 (DLP). (*A*) Retinotopic organization of the ventral areas of the left hemisphere of subject M1. (*B*) Slope estimates (mean and SEM across subjects) between eccentricity and pRF size in dorsal and ventral areas.

V3d. Our results confirm the existence of a V3d (R1) in macaque monkeys. A New World monkey DM would require a combination of R1 (V3d) with R3+ (V3A+) (*SI Appendix*, Fig. S1*D*) or R1 with the posterior part of R3 (*SI Appendix*, Fig. S4 *B* and *C*). However, R1 and R3+, or R1 and the posterior part of R3, have different visual field representations (mirror vs. nonmirror image) and pRF sizes and thus are unlikely parts of the same retinotopic area. According to figure 2 of Rosa and Tweedale (8) and figure 1B of Jeffs et al. (5), the progression of eccentricity is the same in both DM− and DM+, whereas the polar angle progression is reversed along a caudo-rostral axis. Hence, the visual field representation is also different in DM− and DM+ in the marmoset model, exactly as in R1 and R3+. DM in the model of Kaas et al. (4) and Kaas and coworkers (27) (Fig. 1*E*), however, is more similar to R3 (V3A), and their V3d corresponds well to R1 (see also *Discussion*, *V3A*).

A putative marmoset model also requires merging R2− (DLP−) with V3v since V3v alone would then constitute an improbable area in which only one quadrant is represented (2, 8, 15). R2 (DLP) contains the same mirror image representation as V3v; however, its pRF size is significantly larger than V3v. This result, although seemingly in conflict with the marmoset model having a similar receptive field (RF) size in ventral and dorsal VLP (15) (see *SI Appendix* for further discussion), is quite consistent with results in macaques describing a posteromedial area (PM) (28). This area resembles R2− (DLP−) and its RF size equals V4. Thus, in macaque monkeys, converging evidence suggests that R2 (DLP) is a higher-level area distinct from V3v.

However, unlike macaque models 1 and 5, our V3d is reduced in size and borders V2d only anteromedially. The central part of V3d from macaque models 1 and 5 belongs to another area, DLP. This organization, despite being a departure from the traditional macaque model, is in fact largely compatible with connectivity data. First, it fits with connectivity evidence from Lyon and Kaas (17) confirming V3d in macaque monkeys, since all tracer injections were made at eccentricities >5°. It also fits with anatomical data from marmosets suggesting that VLP− and DM− are different areas (5). Second, the new model explains connectivity results in macaques that cannot be accounted for by the old macaque models (1, 5). Specifically, a series of tracer injections in V2d resulted in two separate projection fields immediately rostral to V2d (29). The dorsomedial projection field (their DM−) is very similar to our V3d, since its ventral extension ends at the anterior V2 border near 2° eccentricity and a similar center of gaze is represented at its ventral tip, as corroborated by our results. This result is difficult to reconcile by macaque models 1 and 5, since an elongated V3d would result in duplication of the same visual field in the same area. Finally, in a study by Ungerleider et al. (30), a series of tracers injected at different eccentricities in V4 yielded a topographically organized connectivity pattern in V3d with a clear separation between central and peripheral projections from V4 to V3d. Furthermore, there is a clear difference in laminar distribution of labeled cells and terminals in V3d after central versus peripheral V4 injections, with the latter projections consistently classified as "feedback", whereas those identified after central injections being of the "intermediate" type (see their table 2). This distinction cannot be explained by macaque models 1 and 5, since a homogeneous distribution of laminar projection patterns should be expected in a single area. However, such projection pattern is consistent with our results where DLP and V3d are different areas separated by a gap. Thus, it is conceivable that the central portion of DLP has previously been misassigned to area V3d.

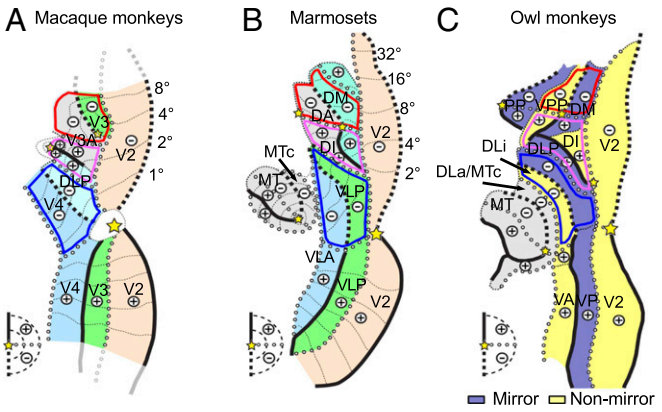

Fig. 6. Comparison Old and New World monkeys. (*A*) Our results. (*B* and *C*) The most recent maps of New World marmoset (*B*) and owl monkeys (*C*). (*B*) Republished with permission of Royal Society, from ref. 8; permission conveyed through Copyright Clearance Center, Inc. (*C*) Modified from ref. 3.

V3A. Rostral and ventral to V3d, we observed another third-tier area (V3A, R3) occupying most of the annectant gyrus and with larger pRF size than V3, highly similar to the initial description given by Van Essen and Zeki (7). However, unlike the rather complex retinotopic organization described by Van Essen and Zeki (7), we observed a single, slightly warped but orderly representation of the entire contralateral hemifield in this area. The retinotopic organization of R3 (V3A) also resembles DM in the model of Kaas and coworkers (17) (Fig. 1*E*), except that R3 abuts V2d directly at eccentricities smaller than 5°. Kaas and coworkers (17) only made injections beyond 5° to define DM; hence the portion of DM touching V2d may have been overlooked.

Macaque model 1 (Fig. 1*A*), however, describes a different V3A, whereby the UVF representation borders V3d posteriorly, near the narrow V3d zone, whereas the LVF representation borders V4 anteriorly. This arrangement is significantly different from our observations and those of Van Essen and Zeki (7), but may be explained if one combines peripheral DLP with the UVF representation of our V3A (R3+) (Fig. 2*C*). Exactly as with V3A of Gattass et al. (6), this combination of quarter fields is located mainly at the anterior bank of the lunate sulcus, largely avoiding the annectant gyrus. Moreover, we observed significant differences in field sign and pRF size between R2+ and R3+, indicating that they belong to separate areas.

V3A as described by Gattass et al. (6) was reported in a study (31) when recordings were made in the annectant gyrus. However, the result may have been misinterpreted due to the complex folding of the annectant gyrus (*SI Appendix*, Fig. S7). In another single-cell recording study (32), the described V3A resembles our results. Therefore, V3A as we observed also fits the literature more closely than suggested by macaque model 1.

V4. Anterior to DLP and V3v, we observed a nonmirror image area sharing a vertical meridian (VM) and a HM with posterior and anterior areas, respectively, very similar to area V4 as described in macaque model 1. Since V4 has been widely accepted in this form, we followed this designation here. However, in its original description by Zeki (33), "V4" referred to a "fourth visual complex" including multiple areas: one located in the anterior bank of the lunate sulcus and another extending from the anterior bank of the lunate sulcus onto the prelunate gyrus. The location of the former area is very similar to our DLP, and the latter fits the dorsal portion of our V4 (V4d). These two areas were grouped since the properties of the cells in these two areas were very similar (33). Consistently, we observed similar pRF sizes in DLP and V4. The combination of V4d and DLP conforms to the same retinotopic organization as observed for the V4 complex by Van Essen and Zeki (7) since they described an UVM representation at the V3A/V4-complex border and the same visual field represented twice in the V4 complex. Therefore, we suggest that DLP and V4 of the present study are parts of Zeki's V4 complex.

Our results are also consistent with several studies describing areas PM and AL (anterolateral) around the macaque prelunate gyrus (28, 34). These two areas are separated by a LVM, and their neurons have the same RF size, exactly as we found in DLP and V4d. The main difference is the UVF representation in DLP, which is lacking in PM, although the authors claim it is present just outside PM's border (28).

Our observation of two dorsal fourth-level visual areas around the prelunate gyrus also fits the connectivity results observed by Kaas and coworkers (27, 29) in macaques (Fig. 1*E*) and the dorsal halves of VLP and VLA in marmosets (Fig. 1*B*). Kaas and coworkers (27, 29) described two distinct projection fields from the anterior bank of the lunate sulcus onto the prelunate gyrus after tracer injections in V2. These two projection fields are similar to V4 and V4A observed by Zeki (35) after lesions made in V2 and V3, but were designated DLc and DLr following the terminology used in New World monkeys. These results, however, are inconsistent with connectivity results observed by Gattass et al. (36), who observed a single projection field in their V4d after injections of tracers in V2d (except their case 8). Different definitions of area V3 and V3A have likely caused discrepant interpretations of these studies. According to our results, area V3A and the central portion of V3d in the macaque model of Gattass et al. (1, 6) correspond to our DLP or the dorsal portion of DLc, whereas Gattass' area V4d corresponds to our V4d or the dorsal portion of DLr. Therefore, it is unsurprising that Gattass et al. observed only a single projection field in their V4d, as they probably assigned the other projection field to other areas (e.g., V3A).

The ventral fourth-level visual area, however, differs from that proposed by Kaas and coworkers (27, 29), as we observed only a ventral counterpart for V4d (quarter field) and obviously not for DLP (which is already a hemifield), while Kaas et al. described upper field quadrants for both DLc and DLr (Fig. 1*E*). Zeki (35) also described two projection fields from V2v and V3v immediately rostral to V3v, i.e., V4 and V4A. These regions correspond to our V4v and another mirror image area rostral to V4v, which we have also named V4A in our previous study (13) (see also refs. 14 and 37). These two areas are very similar to the ventral portions of DLc and DLr (27, 29). However, V4v and V4A cannot be considered as the ventral counterparts of DLP and V4d, respectively, since their visual fields are entirely different (i.e., mirror versus nonmirror image representations). It is possible that these areas are incorrectly combined by Kaas et al. (27, 29) and Zeki (35) since their detailed visual topography (especially polar angle representation) is difficult to discern based on connectivity patterns only. Furthermore, Zeki (33) grouped V4 and V4A together based on the spike data from their dorsal portions, which in fact correspond to our DLP and V4d. Whether V4A can be considered as another fourth-level visual area is still an open question.

Comparison Old and New World Monkeys. Fig. 6*A* summarizes the overall retinotopic organization of the third and fourth visual areas whereby different quadrant representations were grouped based on visual field representation and receptive field size. A direct comparison of our results (Fig. 6*A*) with the most recent maps of New World marmoset and owl monkeys (Fig. 6 *B* and *C*) revealed remarkably similar visuotopic representations in the dorsal visual cortex. Within 12° of eccentricity, two HM representations are connected perpendicularly with the HM constituting the rostral V2d border in each species. These HMs separate the visual cortex immediately rostral to V2d into three zones: a medial (red outline) and lateral (blue outline) LVF separated by an UVF zone (pink outline). The medial LVF zone is characterized by a LVM in each species, splitting V3d– from V3A– in macaques, DM– from VPP– in owl monkeys, and DM– from DA– in marmosets. The UVF zone has a complicated visual field organization, leading to distinct partitioning schemes in different species. However, an UVM is observed in each species separating two sets of upper quadrant

representations (i.e., DLP+ in macaque and owl monkeys and DI+ in marmosets, separated from V3A+ in macaques; DI+, DM+, and VPP+ in owl monkeys; and DM+ and DA+ in marmosets). The most lateral zone contains a double representation of the contralateral LVF in all species. A LVM represents the anterior border of the posterior lower quadrant (DLP− in macaque and owl monkeys, and VLP− in marmosets) shared with another fourth-level visual area located more rostrally (V4d in macaques and the V4-like areas DLi and VLA in owl monkeys and marmosets, respectively). In addition to the meridians, (near) foveal representations can be retrieved at highly similar topographic locations relative to the medial HM in each species. Hence, the general visual topographic organization of the dorsal visual cortex exhibits surprisingly more similarity in Old and New World monkeys than was previously appreciated.

In conclusion, our results reveal a retinotopic organization of the dorsal visual cortex in macaques that substantially differs from currently most prevailing models. Although individual quadrants are well defined, it remains challenging to group them into hemifields. We relied on field sign information and intrinsically noisy pRF data for our current interpretation regarding areal definitions. Other schemes, however, might be considered using different grouping criteria (see *SI Appendix* for detailed discussions). However, the proposed model reconciles most reported discrepancies concerning the visuotopic organization of the nonhuman primate caudo-dorsal occipital cortex. Hence, our model (Fig. 6*A*) provides a plausible explanation of all data. The overall visuotopic organization of these areas is remarkably similar in Old and New World monkeys, suggesting that this organization is evolutionarily preserved. Future multimodal studies guided by our maps, including measurements of anatomical connectivity and RF properties at the single-cell level, will eventually lead to an optimized and fully conclusive parcellation model. Also, high-resolution imaging is required to ascertain whether a similar organization may exist in humans, as was implied, but not discussed, in the very first phase-encoded retinotopic mapping study of Sereno et al. (38) (their figure 3) (see *SI Appendix* for further discussions).

Methods

Three monkeys were scanned using phase-encoded retinotopic mapping methods (38). Runs of data (127/50 and 75/48) covering the top/bottom part of the brain of two subjects (M1 and M3, respectively) were collected in separate sessions. Fifty-six runs of data covering the whole brain were collected from the third subject (M2). A conventional Fourier-based method (38) was conducted to calculate polar angle and eccentricity maps, from which the iso-polar angle and iso-eccentricity contour lines and visual field sign maps were calculated to reveal fine-grained visual field representation of the cortex immediately anterior to macaque V2d. Furthermore, pRF sizes (21) were analyzed to quantitatively evaluate different parcellation models. Full details of acquisition and analysis procedures can be found in *SI Appendix*. Animal care and experimental procedures were performed in accordance with the National Institute of Health's *Guide for the Care and Use of Laboratory Animals* (39), the European legislation (Directive 2010/63/EU) and were approved by the Ethical Committee of KU Leuven.

ACKNOWLEDGMENTS. We thank A. Coeman, C. Fransen, P. Kayenbergh, I. Puttemans, S. De Pril, A. Hermans, G. Meulemans, W. Depuydt, C. Ulens, S. Verstraeten, and M. Depaep for technical and administrative support; and Dr. S. Raiguel, Dr. D. Van Essen, and Dr. M. Glasser for their comments on the manuscript. This work was supported by Research Foundation Flanders (FWO-Flanders) Grants G0B8617N, G0D5817N, G0A5613N, and Odysseus G0007.12; KU Leuven Programme Financing Grants PFV/10/008 and C14/17/109; and European Union's Horizon 2020 Framework Programme for Research and Innovation under Grant Agreement 785907 (Human Brain Project SGA2).

1. Gattass R, Lima B, Soares JGM, Ungerleider LG (2015) Controversies about the visual areas located at the anterior border of area V2 in primates. *Vis Neurosci* 32:E019.
2. Angelucci A, Rosa MGP (2015) Resolving the organization of the third tier visual cortex in primates: A hypothesis-based approach. *Vis Neurosci* 32:E010.
3. Sereno MI, McDonald CT, Allman JM (2015) Retinotopic organization of extrastriate cortex in the owl monkey: Dorsal and lateral areas. *Vis Neurosci* 32:E021.
4. Kaas JH, Roe AW, Baldwin MKL, Lyon DC (2015) Resolving the organization of the territory of the third visual area: A new proposal. *Vis Neurosci* 32:E016.
5. Jeffs J, Federer F, Angelucci A (2015) Corticocortical connection patterns reveal two distinct visual cortical areas bordering dorsal V2 in marmoset monkey. *Vis Neurosci* 32:E012.
6. Gattass R, Sousa AP, Gross CG (1988) Visuotopic organization and extent of V3 and V4 of the macaque. *J Neurosci* 8:1831–1845.
7. Van Essen DC, Zeki SM (1978) The topographic organization of rhesus monkey prestriate cortex. *J Physiol* 277:193–226.
8. Rosa MG, Tweedale R (2005) Brain maps, great and small: Lessons from comparative studies of primate visual cortical organization. *Philos Trans R Soc Lond B Biol Sci* 360:665–691.
9. Janssens T, et al. (2012) An implanted 8-channel array coil for high-resolution macaque MRI at 3T. *Neuroimage* 62:1529–1536.
10. Li X, Zhu Q, Janssens T, Arsenault JT, Vanduffel W (2019) In vivo identification of thick, thin, and pale stripes of macaque area V2 using submillimeter resolution (f)MRI at 3 T. *Cereb Cortex* 29:544–560.
11. Vanduffel W, et al. (2001) Visual motion processing investigated using contrast agent-enhanced fMRI in awake behaving monkeys. *Neuron* 32:565–577.
12. Brewer AA, Press WA, Logothetis NK, Wandell BA (2002) Visual areas in macaque cortex measured using functional magnetic resonance imaging. *J Neurosci* 22:10416–10426.
13. Janssens T, Zhu Q, Popivanov ID, Vanduffel W (2014) Probabilistic and single-subject retinotopic maps reveal the topographic organization of face patches in the macaque cortex. *J Neurosci* 34:10156–10167.
14. Arcaro MJ, Livingstone MS (2017) Retinotopic organization of scene areas in macaque inferior temporal cortex. *J Neurosci* 37:7373–7389.
15. Rosa MG, Tweedale R (2000) Visual areas in lateral and ventral extrastriate cortices of the marmoset monkey. *J Comp Neurol* 422:621–651.
16. Lyon DC, Kaas JH (2001) Connectional and architectonic evidence for dorsal and ventral V3, and dorsomedial area in marmoset monkeys. *J Neurosci* 21:249–261.
17. Lyon DC, Kaas JH (2002) Evidence for a modified V3 with dorsal and ventral halves in macaque monkeys. *Neuron* 33:453–461.
18. Allman JM, Kaas JH (1975) The dorsomedial cortical visual area: A third tier area in the occipital lobe of the owl monkey (Aotus trivirgatus). *Brain Res* 100:473–487.
19. Rosa MGP, Schmid LM (1995) Visual areas in the dorsal and medial extrastriate cortices of the marmoset. *J Comp Neurol* 359:272–299.
20. Van Der Gucht E, Youakim M, Arckens L, Hof PR, Baizer JS (2006) Variations in the structure of the prelunate gyrus in Old World monkeys. *Anat Rec A Discov Mol Cell Evol Biol* 288:753–775.
21. Dumoulin SO, Wandell BA (2008) Population receptive field estimates in human visual cortex. *Neuroimage* 39:647–660.
22. Gattass R, Gross CG, Sandell JH (1981) Visual topography of V2 in the macaque. *J Comp Neurol* 201:519–539.
23. Desimone R, Schein SJ (1987) Visual properties of neurons in area V4 of the macaque: Sensitivity to stimulus form. *J Neurophysiol* 57:835–868.
24. Boussaoud D, Desimone R, Ungerleider LG (1991) Visual topography of area TEO in the macaque. *J Comp Neurol* 306:554–575.
25. Rosa MGP, Fritsches KA, Elston GN (1997) The second visual area in the marmoset monkey: Visuotopic organisation, magnification factors, architectonical boundaries, and modularity. *J Comp Neurol* 387:547–567.
26. Piñon MC, Gattass R, Sousa AP (1998) Area V4 in Cebus monkey: Extent and visuotopic organization. *Cereb Cortex* 8:685–701.
27. Stepniewska I, Collins CE, Kaas JH (2005) Reappraisal of DL/V4 boundaries based on connectivity patterns of dorsolateral visual cortex in macaques. *Cereb Cortex* 15: 809–822.
28. Maguire WM, Baizer JS (1984) Visuotopic organization of the prelunate gyrus in rhesus monkey. *J Neurosci* 4:1690–1704.
29. Stepniewska I, Kaas JH (1996) Topographic patterns of V2 cortical connections in macaque monkeys. *J Comp Neurol* 371:129–152.
30. Ungerleider LG, Galkin TW, Desimone R, Gattass R (2008) Cortical connections of area V4 in the macaque. *Cereb Cortex* 18:477–499.
31. Nakamura K, Colby CL (2002) Updating of the visual representation in monkey striate and extrastriate cortex during saccades. *Proc Natl Acad Sci USA* 99:4026–4031.
32. Galletti C, Battaglini PP (1989) Gaze-dependent visual neurons in area V3A of monkey prestriate cortex. *J Neurosci* 9:1112–1125.
33. Zeki SM (1978) Functional specialisation in the visual cortex of the rhesus monkey. *Nature* 274:423–428.
34. Youakim M, Bender DB, Baizer JS (2001) Vertical meridian representation on the prelunate gyrus in area V4 of macaque. *Brain Res Bull* 56:93–100.
35. Zeki SM (1971) Cortical projections from two prestriate areas in the monkey. *Brain Res* 34:19–35.
36. Gattass R, Sousa AP, Mishkin M, Ungerleider LG (1997) Cortical projections of area V2 in the macaque. *Cereb Cortex* 7:110–129.
37. Pigarev IN, Nothdurft H-C, Kastner S (2002) Neurons with radial receptive fields in monkey area V4A: Evidence of a subdivision of prelunate gyrus based on neuronal response properties. *Exp Brain Res* 145:199–206.
38. Sereno MI, et al. (1995) Borders of multiple visual areas in humans revealed by functional magnetic resonance imaging. *Science* 268:889–893.
39. National Research Council (2011) *Guide for the Care and Use of Laboratory Animals* (National Academies Press, Washington, DC), 8th Ed.